ACS APPLIED BIO MATERIALS

www.acsabm.org Article

Visible Fluorescent Light-up Probe for DNA Three-Way Junctions Provides Host–Guest Biosensing Applications

Abigail J. Van Riesen, Jennifer Le, Sladjana Slavkovic, Zachary R. Churcher, Aron A. Shoara, Philip E. Johnson,* and Richard A. Manderville*

Cite This: *ACS Appl. Bio Mater.* 2021, 4, 6732–6741 Read Online

ACCESS | Metrics & More | Article Recommendations | Supporting Information

ABSTRACT: DNA three-way junctions (3WJs) consist of a Y-shaped hydrophobic branch point connecting three double-stranded stems and are viewed as druggable targets for cancer treatment. They are also important building blocks for the construction of DNA nanostructures and serve as recognition elements for DNA aptasensors for a wide variety of diagnostic applications. However, visible fluorescent light-up probes for specific staining of DNA 3WJs are currently lacking. Herein, we report that a merocyanine containing the *N*-methylbenzothiazolium (Btz) acceptor vinyl linked to a 2-fluorophenolic (FPhO) donor (FPhOBtz) serves as a universal fluorescent turn-on dye for DNA 3WJs. Our evidence is based on a multifaceted approach to define the specificity and affinity of FPhOBtz for 3WJ DNA aptamers; the cocaine binding aptamer MN4, the cholic acid binding aptamer (CABA), and four steroid aptamers (DOGS.1, DISS.1, BES.1, DCAS.1). FPhOBtz exhibits impressive turn-on (up to 730-fold) fluorescence at 580 nm upon aptamer binding with low micromolar affinity. Direct FPhOBtz displacement from the 3WJ binding domain through competitive alkaloid and steroid binding provides immediate fluorescent read out for host–guest detection strategies in human blood serum in the low micromolar regime. Our results present the first visible light-up fluorescent probe for DNA 3WJ detection strategies.

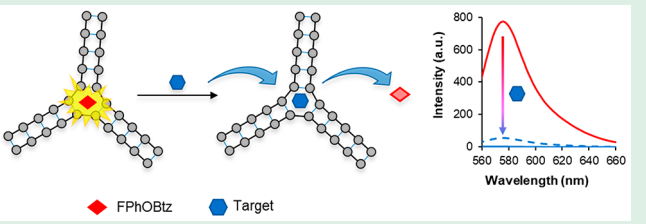

KEYWORDS: *DNA three-way junctions, fluorescent probe, merocyanine, host–guest detection, cocaine, quinine*

INTRODUCTION

DNA three-way junctions (3WJs) are unique branched structures consisting of three double-stranded stems connected by a triangular-shaped hydrophobic branch point.[1] They are produced during DNA replication and are viewed as druggable targets through creation of 3WJ-specific agents that can stabilize the structure to promote cell death in proliferating cancer cells.[2] The branched DNA 3WJ is also an important building block for the construction of DNA nanostructures[3,4] and serves as a motif for the creation of aptamer-based sensors (aptasensors)[5,6] for binding proteins,[7] small-molecule targets,[8,9] and even cells.[10]

A simple aptasensor uses fluorescent light-up probes that bind specific DNA topologies in a label-free platform that does not require chemical modification of the aptamer.[4,11] Numerous label-free platforms have been developed for the G-quadruplex (GQ) motif that is also a common recognition element for aptasensors.[11−13] The platforms typically rely on structure switching,[14] which may involve a GQ–duplex equilibrium or a GQ–GQ nanodevice due to the polymorphic nature of GQs.[13] Both the duplex and GQs provide a stacking surface for π-extended visible chromophores, such as commercially available thiazole orange (TO),[15] Thioflavin T (ThT),[16] and SYBR Green I (SGI).[17] These dyes exhibit strongly quenched fluorescence when free in solution due to torsional twisting and dye–dye contact.[18] However, they can exhibit >1000-fold emission enhancement upon binding DNA.[15−17] Target-mediated dye displacement from the aptamer provides a fluorescence read out.

Label-free platforms for 3WJ aptamers are rare, as the dye should recognize the Y-shaped branch point and undergo displacement through competitive target binding in the absence of structure switching.[6] Examples include the use of a blue cyanine (Cy7) colorimetric indicator that undergoes color fading upon target addition[19] and a more sensitive fluorescent-based assay with a naphthyridine (ATMND) probe that exhibits UV emission at 405 nm with quenched fluorescence upon 3WJ binding.[20] A calix[3]carbazole also displays 3WJ binding specificity but possesses UV emission at 389 nm with macrocycle aggregation.[21]

Herein, we demonstrate specific 3WJ DNA binding by merocyanine (FPhOBtz, Figure 1) containing the *N*-methylbenzothiazolium (Btz) acceptor vinyl linked to the 2-

Received: April 10, 2021
Accepted: August 5, 2021
Published: August 18, 2021

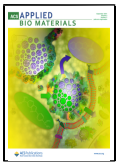

https://doi.org/10.1021/acsabm.1c00431
ACS Appl. Bio Mater. 2021, 4, 6732–6741

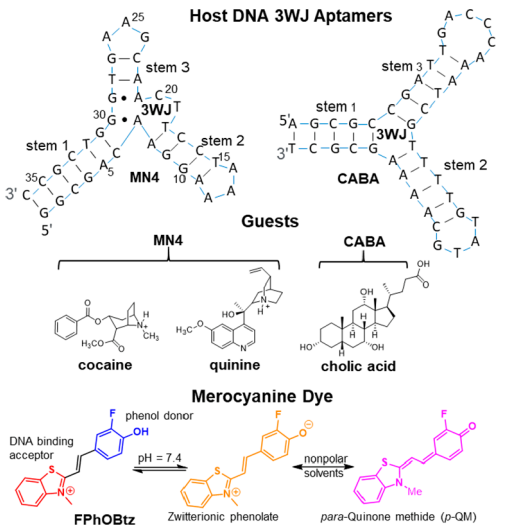

Figure 1. Structures of host 3WJ aptamers (cocaine binding aptamer (MN4) and cholic acid aptamer (CABA)), alkaloid, and bile acid guests, and features of the merocyanine dye FPhOBtz.

fluorophenolic (FPhO) donor. While Btz is a classic DNA binding motif in fluorescent light-up probes,[13,15−17] negatively charged phenolate donors are not commonly employed for DNA staining. Instead, they serve as pH indicators[22] and as solvent polarity probes due to their impressive negative solvatochromism.[23] This latter feature stems from the dye's preference for the zwitterionic form in water that switches to the more rigid neutral *p*-quinone methide (*p*-QM) resonance structure in nonpolar solvents (Figure 1). The phenolate possesses spectacular solvatochromic properties and appears to be well suited for sensing the hydrophobic branch point of DNA 3WJs as *p*-QM formation can provide a fluorescent readout signal. Hence, to optimize dye response, the ortho-F atom was added to lower the phenolic pK_a (the unsubstituted PhOHBtz has a pK_a ≈ 8.0[23]) and promote phenolate formation at pH 7.4. The 3WJ binding specificity of FPhOBtz is initially demonstrated in two host DNA 3WJ aptamers: the cocaine-binding aptamer MN4[24,25] and the cholic acid binding aptamer (CABA, Figure 1).[26,27] The 3WJ within MN4 contains a dynamic 3WJ binding site, which exhibits ligand binding promiscuity and interacts with other alkaloids, such as quinine, with higher affinity than its intended cocaine target.[28] In contrast, CABA contains a tight 3WJ with canonical Watson−Crick (W−C) base pairs. Four additional 3WJ aptamers that specifically bind steroids were then examined to establish FPhOBtz as a universal 3WJ binding probe. Our findings are the first to report selective sensing of the DNA 3WJ motif by a visible fluorescent light-up dye and highlight host−guest detection with sensitivity that rivals label-free GQ detection platforms.

RESULTS AND DISCUSSION

FPhOBtz Binding to MN4 and CABA. In aqueous buffer FPhOBtz possesses a pK_a ≈ 6.6 with phenol and phenolate absorbance at ∼398 (ε = 32 787 cm^{-1} M^{-1}) and ∼485 nm (ε = 34 636 cm^{-1} M^{-1}) (Figure S1A, Supporting Information (SI)). In protic solvents (H_2O, MeOH, EtOH, and IPA), the dye displays negative solvatochromism with progressive absorbance shifts to the red with decreased solvent polarity (MeOH, ε_{526} = 48 864 cm^{-1} M^{-1}; EtOH ε_{548} = 64 428 cm^{-1} M^{-1}; IPA, ε_{556} = 82 077 cm^{-1} M^{-1}, Figure S2A). The λ_{max} values provided a linear correlation with the empirical solvent polarity scale E_T(30) (Figure S2B).[29]

A UV−vis titration of the dye (5 μM) with MN4 (Figure 2A) also displays an impressive red shift with a distinct color

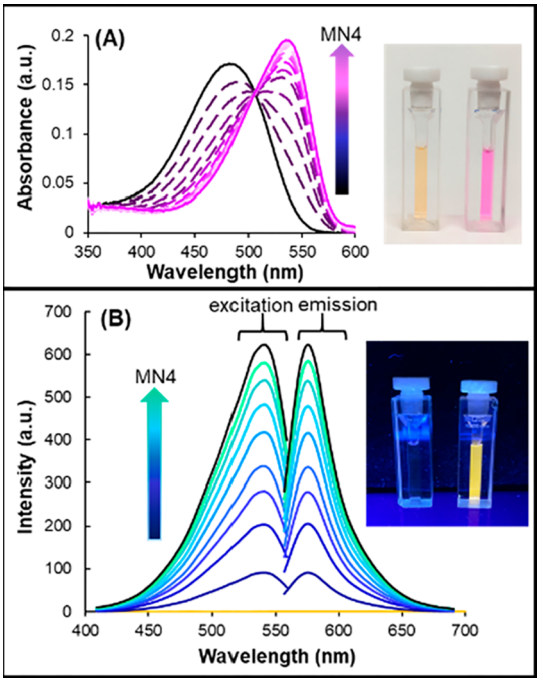

Figure 2. (A) UV−vis titration of 5 μM FPhOBtz (black trace) with MN4 (0.2 equiv additions); (inset) cuvettes containing free FPhOBtz (pale orange solution) and with 4 equiv of MN4 (deep pink solution). (B) Fluorescence titration of 1 μM FPhOBtz (solid yellow trace) with MN4 (0.25 equiv additions); (inset) cuvettes containing free FPhOBtz (no fluorescence) and with 2.25 equiv of MN4 (bright yellow fluorescence). Titrations were carried out in PBS pH 7.4 at 25 °C.

change from 485 (free dye, black trace) to 540 nm (purple trace, $\Delta\lambda_{max}$ = 55 nm) with increased absorbance (ε ≈ 39 000 cm^{-1} M^{-1}). The titration afforded an apparent dissociation constant (K_d) of 2.63 ± 0.2 μM. The λ_{max} value for DNA-bound FPhOBtz approaches its λ_{max} in EtOH and provided an E_T(30) value of ∼52.5 kcal/mol (Figure S2B), which is considerably lower than that of water (E_T(30) = 63.1 kcal/mol). Clearly, FPhOBtz binding to MN4 causes concealment of the dye from the bulk aqueous solvent.

The fluorescence response of FPhOBtz to MN4 binding was truly impressive, providing a >600-fold emission intensity increase at ∼580 nm to provide bright yellow fluorescence (Figure 2B). In PBS at pH 7.4, free FPhOBtz provided a fluorescence quantum yield (Φ_{fl}) of 0.085 for a brightness ($\varepsilon\Phi_{fl}$) of 2944 M^{-1} cm^{-1}. For the MN4·FPhOBtz complex, Φ_{fl} = 0.76 for $\varepsilon\Phi_{fl}$ = 26 640 M^{-1} cm^{-1}, a 10-fold increase in brightness compared to free FPhOBtz in PBS. For comparison, the brightness of PicoGreen dye (ε ≈ 70 000 cm^{-1} M^{-1}) bound to calf thymus DNA (Φ_{fl} ≈ 0.5) is ∼35 000 cm^{-1} M^{-1},[30] which is only 1.3-fold brighter than the MN4·FPhOBtz complex. The emission intensity response was also pH dependent, exhibiting an ∼3.5-fold increase at 580 nm upon raising the pH from 6.0 to 8.5 (Figure S3). Thus, increased dye rigidity coupled with the phenolate that can produce the *p*-QM

https://doi.org/10.1021/acsabm.1c00431
ACS Appl. Bio Mater. 2021, 4, 6732−6741

resonance structure was deemed important for the emission intensity response of FPhOBtz binding to MN4.

The optical response of FPhOBtz to other 3WJ aptamers was initially tested using CABA (Figure 3). A UV−vis titration

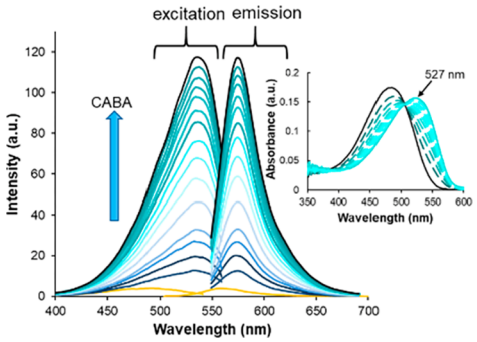

Figure 3. UV−vis (insert) and fluorescence spectral changes of FPhOBtz upon binding CABA. For the UV−vis titration, FPhOBtz (5 μM, black trace, insert) was titrated with CABA (1.0 equiv additions up to 13 equiv, turquoise traces). Fluorescence titration of 1 μM FPhOBtz (solid yellow trace) with CABA (0.20 equiv additions up to 3 equiv). Titrations were carried out in PBS pH 7.4 at 25 °C.

of the dye (5 μM) with CABA (insert, Figure 3) also displayed a red shift from 485 (free dye, black trace) to 527 nm (turquoise traces, $\Delta\lambda_{max}$ = 42 nm) but with decreased absorbance ($\varepsilon \approx 31\,200$ cm^{-1} M^{-1}) and afforded a higher K_d value of 12.4 ± 1.0 μM compared to FPhOBtz binding to MN4 (4.7-fold increase in K_d). An $E_T(30)$ value of ∼55.1 kcal/mol (Figure S2B) was determined, which is similar to the value for MeOH ($E_T(30)$ = 55.4 kcal/mol).[29] The fluorescence intensity increase of FPhOBtz binding to CABA was also impressive, >100-fold at ∼580 nm.

Isothermal titration calorimetry (ITC) was also utilized to derive aptamer binding constants for FPhOBtz under conditions previously employed for guest binding to MN4 (Figure 4, Table 1). Titration of FPhOBtz into the MN4 aptamer (Figure 4A) shows that binding is exothermic with a dissociation constant (K_d) of 0.42 μM (Table 1) at 15 °C. The sigmoidal shape of the thermogram indicates that binding is single-sited at 140 mM NaCl as observed previously with cocaine and quinine[31] and not two-sited as observed for amodiaquine and mefloquine.[32] As a positive control, titration of quinine into MN4 aptamer was performed, and the obtained results agree with the previously published data (Table 1; Figure S4).[28,33] The binding of cocaine, quinine, and FPhOBtz to the MN4 aptamer all have an unfavorable binding entropy and display enthalpically driven binding,[28,34] consistent with a similar binding mode for these ligands.

The thermogram for FPhOBtz binding to CABA (Figure 4B) indicates that binding is single-sited, with a K_d value of 9 μM. For comparison, titration of cholic acid into CABA was also performed (Figure S5) with the binding parameters provided in Table 1. Our measured affinity of cholic acid for CABA (24 μM) is consistent with the previously reported value of 19.6 μM.[35] The similarity in binding thermodynamics for FPhOBtz to both MN4 and CABA indicated the likelihood of similar interactions between the dye and the two aptamers (Table 1).

3WJ Binding Specificity by FPhOBtz and Target-Mediated Displacement. To provide information on the location of the binding site of FPhOBtz in the MN4 aptamer,

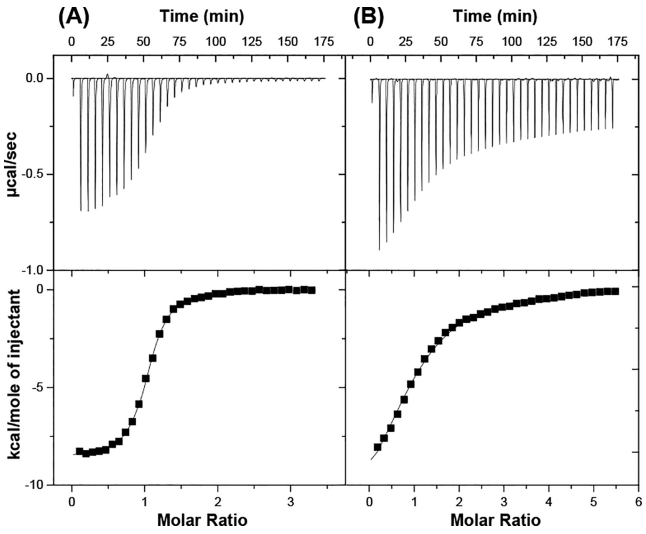

Figure 4. ITC thermograms showing binding of FPhOBtz to (A) the MN4 cocaine binding aptamer and (B) the cholic acid binding aptamer (CABA). (Top) Raw titration data showing the heat resulting from each injection of ligand into the aptamer solution. (Bottom) Integrated heat plot after correcting for the heat of dilution. Data for MN4 binding was acquired in 20 mM Tris (pH 7.4), 140 mM NaCl, 5 mM KCl with the addition of 1% (v/v) DMSO at 15 °C. Data for CABA binding was acquired in 10 mM sodium phosphate (pH 7.4), 140 mM NaCl, 5 mM KCl with the addition of 1% (v/v) DMSO at 15 °C.

Table 1. ITC Binding Affinity and Thermodynamic Parameters of Ligand Binding to MN4 and CABA[a]

ligand	K_d (μM)	ΔH (kcal/mol)	$-T\Delta S$(kcal/mol)
MN4 cocaine binding aptamer			
cocaine[b]	5.5 ± 0.4	−11 ± 1	4 ± 1
quinine	0.21 ± 0.02	−14 ± 1	5 ± 1
FPhOBtz	0.42 ± 0.01	−9.3 ± 0.5	0.9 ± 0.5
cholic acid binding aptamer (CABA)			
CA	24 ± 3	−6.4 ± 0.2	0.3 ± 0.1
FPhOBtz	9 ± 3	−14 ± 3	7 ± 3

[a]Values reported are averages of 2−3 individual experiments. [b]Data taken from ref 25. Binding experiments were performed at 15 °C in 20 mM TRIS (pH 7.4), 140 mM NaCl, 5 mM KCl for MN4 binding and in 10 mM sodium phosphate (pH 7.4), 140 mM NaCl, 5 mM KCl for CABA binding.

dye binding was monitored using 1D ^{1}H NMR spectroscopy. The imino proton region of MN4 is displayed in Figure 5. The free MN4 sample looks very similar to previously reported spectra.[36,37] As FPhOBtz was titrated into the MN4 sample some of the imino proton resonances shifted, consistent with ligand binding. The identities of the imino proton resonances for the FPhOBtz-bound MN4 were confirmed using a 2D NOESY spectroscopy (Figure S6). The connectivity observed with FPhOBtz-bound MN4 is the same as that observed in previous MN4 NOESY experiments with different ligands,[25,36] indicating that MN4 forms a similar structure when bound to FPhOBtz.

The position of the imino protons in MN4 between the free and the FPhOBtz-bound MN4 and their change in chemical shift is provided in Figure S7. The imino protons that change chemical shift most with FPhOBtz binding are T18, T28, G30, and G31 (see Figure 1 for numbering of MN4). These four resonances are all located at or adjacent to the 3WJ of the

https://doi.org/10.1021/acsabm.1c00431
ACS Appl. Bio Mater. 2021, 4, 6732−6741

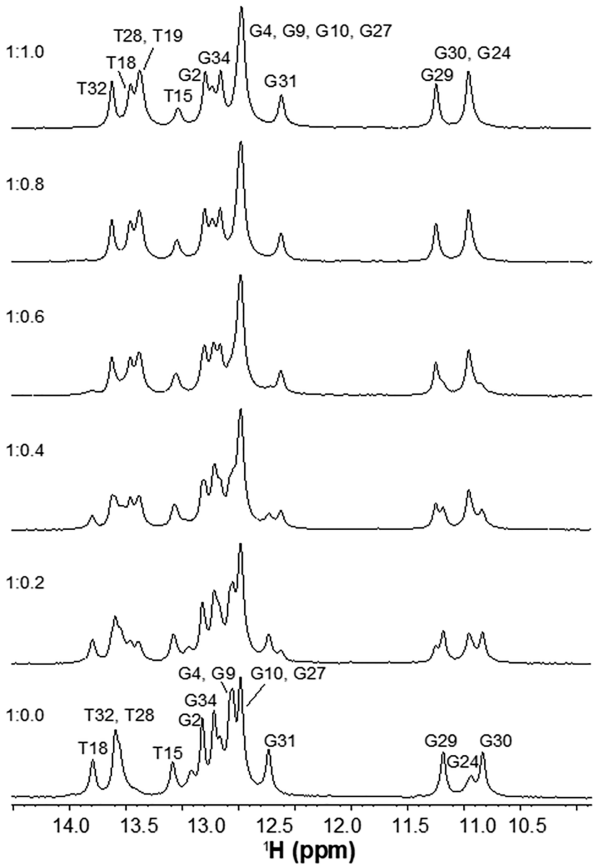

Figure 5. One-dimensional ^{1}H NMR spectra showing the titration of FPhOBtz into the MN4 cocaine binding aptamer. Spectra show the imino proton resonances of the NMR spectra. Ratios on the spectrum denote the molar ratio of aptamer to FPhOBtz. Spectra were acquired with an MN4 concentration of 1.4 mM in 140 mM NaCl, 10 mM $Na_xH_yPO_4$, pH 6.8, 10% $^{2}H_2O$–90% H_2O at 5 °C.

aptamer, which is the high-affinity binding site for cocaine and quinine. The resonances that shift most with FPhOBtz binding are very similar to the resonances that shift most with cocaine binding (G31, T32, T28, and G30)[36] and quinine binding (G31, T18, G24, and G30),[37] suggesting 3WJ binding by the dye. Our multifaceted approach to confirm 3WJ binding specificity by FPhOBtz is critical[38] to establish the dye's potential for host–guest detection, given that the dye possesses greater affinity for the aptamer than two of the intended ligands (cocaine and cholic acid).

The ability of the three guests (cocaine, quinine, and cholic acid) to directly displace FPhOBtz from the 3WJ aptamers was initially investigated using fluorescence intensity measurements (Figure 6, Figure S8). For these experiments FPhOBtz (1 μM) was mixed with 2 equiv of aptamer and ligand binding was assessed through loss of the FPhOBtz emission intensity due to competitive binding by the guest to the 3WJ binding domain. All three ligands were able to cause loss of FPhOBtz emission intensity through dye displacement, which further established 3WJ binding specificity by FPhOBtz. For FPhOBtz displacement from MN4, quinine was much more effective than cocaine at displacing FPhOBtz, requiring 10 equiv of quinine (relative to [FPhOBtz]) to cause a 93% loss of FPhOBtz emission (Figure 6), while 100 equiv of cocaine was required for 86% loss of FPhOBtz fluorescence (Figure S8A). For

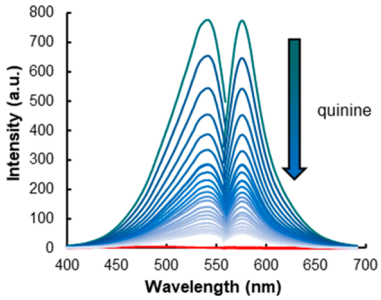

Figure 6. Fluorescence titration of quinine-mediated displacement of FPhOBtz (1 μM) from MN4 (2 μM). Titration with quinine (10 equiv vs [FPhOBtz]) was carried out in PBS pH 7.4 at 25 °C. Red trace is the fluorescence of free FPhOBtz.

FPhOBtz displacement from CABA, 50 equiv of cholic acid caused an 80% loss of FPhOBtz emission (Figure S8B).

From the FPhOBtz emission displacement titrations, a limit of detection (LoD) ≈ 0.13 μM and a limit of quantification (LoQ) = 0.38 μM was determined for quinine (R^2 = 0.99, Figure S9A), while the corresponding LoD values for cocaine and cholic acid were 4.06 (LoQ = 12.3 μM, R^2 = 0.98, Figure S9B) and 0.80 μM (LoQ = 1.38 μM, R^2 = 0.99, Figure S9C), respectively.

ITC-based competition experiments were also carried out. In the first experiment, FPhOBtz was prebound to the cocaine binding aptamer (1.5:1 molar ratio, FPhOBtz:MN4) and quinine was titrated into the solution (Figure 7A). In this case,

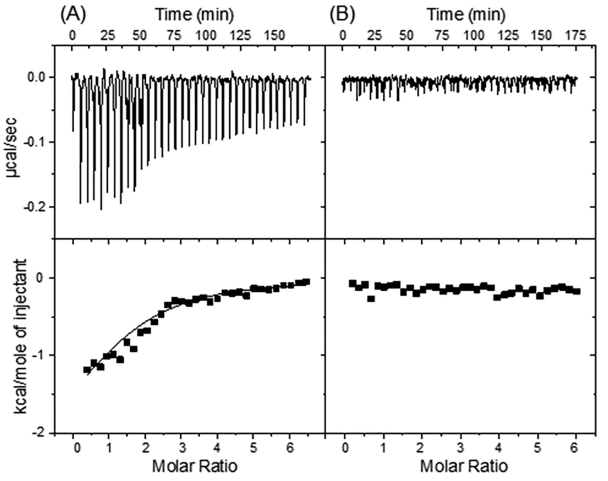

Figure 7. ITC-based competition binding experiments. Interaction of (A) FPhOBtz-bound MN4 with quinine and (B) quinine-bound MN4 with FPhOBtz. (Top) Raw titration data showing the heat resulting from each injection of ligand into the aptamer solution. (Bottom) Integrated heat plot after correcting for the heat of dilution. All binding experiments were performed at 15 °C in a PBS buffer (pH 7.4) containing 0.6% DMSO.

binding by quinine was observed, as the tighter binding quinine displaces FPhOBtz. The data was fit to a competitive binding model, which resulted in a K_d of 0.11 ± 0.03 μM and ΔH of −11 ± 1 kcal/mol (Table S1). Next, a second ITC-based displacement contained quinine prebound to the cocaine binding aptamer (1.5:1 molar ratio, quinine:MN4) and FPhOBtz was titrated into the solution. In this case, no binding was observed for the addition of FPhOBtz into the quinine-bound aptamer (Figure 7B). We conclude that both

https://doi.org/10.1021/acsabm.1c00431
ACS Appl. Bio Mater. 2021, 4, 6732–6741

ligands share a common binding site (3WJ) and that quinine is confirmed as a tighter binding ligand than FPhOBtz. These results support the conclusion that the emission intensity loss of FPhOBtz from quinine addition (Figure 7) was due to dye displacement from the 3WJ binding domain of MN4.

A set of ITC-based competition experiments to determine whether FPhOBtz and cholic acid share the same binding site on the CABA was also performed. In the first experiment, cholic acid was prebound to the CABA (1.5:1 molar ratio, cholic acid:CABA) and then FPhOBtz was titrated into the solution. Binding was observed as the tighter binding ligand, FPhOBtz, displaces cholic acid (Figure S10). Again, data was fit to a competitive binding model which gave a K_d value of 3 ± 1 uM and ΔH of −11 ± 1 kcal/mol (Table S1). In the second experiment, FPhOBtz was prebound to the CABA (1.5:1 molar ratio, FPhOBtz:CABA) and cholic acid was titrated into the mixture. However, under these conditions (20 uM CABA) no detectable binding was observed for the addition of cholic acid into the FPhOBtz−aptamer complex (Figure S10). These results confirm that both cholic acid and FPhOBtz compete for the same binding site on the CABA and that FPhOBtz is the tighter binding ligand (Table 1).

Quinine was also titrated into a sample of MN4−FPhOBtz and tracked with 1D NMR to see if the two ligands compete for the same binding site (Figure 8). In quinine-bound MN4 (top trace, Figure 8), the position of the G31 imino proton resonance is indictive of quinine binding and appears at 11.1 ppm in the bound aptamer,[28] while in FPhOBtz·MN4 the G31 proton is located downfield at 12.2 ppm (1:1:0.00 trace). As quinine was added to the FPhOBtz-bound sample, the G31 imino resonance associated with the FPhOBtz-bound aptamer began to decrease in intensity and the upfield resonance associated with quinine-bound aptamer began to appear (indicated by red dot in Figure 8) as the two states are in slow exchange on the NMR time scale. The downfield G31 resonance continued to shrink in intensity and the upfield resonance grew in intensity as quinine was added until a ratio of 1:1:1 MN4:FPhOBtz:quinine, at which point the FPhOBtz-bound G31 peak had disappeared. The peaks in the final titration point are broadened when compared with the original FPhOBtz-bound MN4 or a sample of quinine-bound MN4. We observed similar broadening in previous NMR competition experiments between cocaine and quinine.[28] Thus, the NMR experiments confirm competitive displacement of MN4-bound FPhOBtz by quinine.

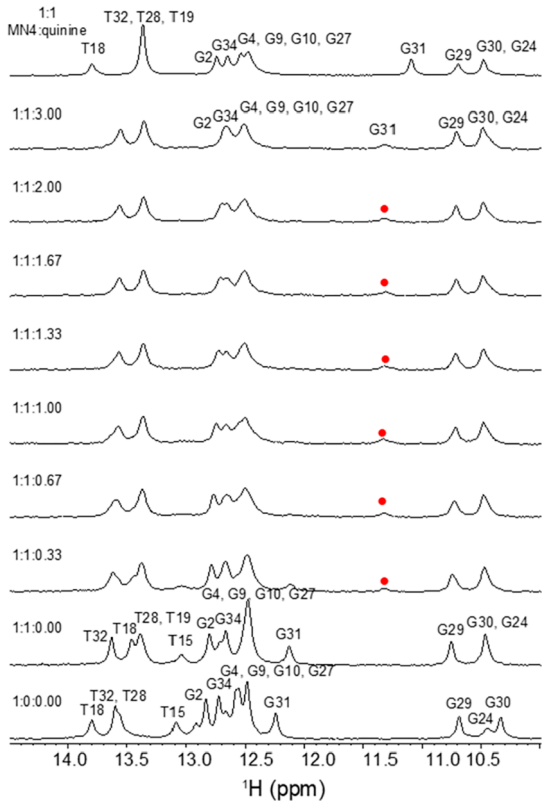

Figure 8. ^{1}H NMR spectra showing the imino proton resonances during a titration of FPhOBtz and quinine into a sample of the MN4 aptamer. Ratios on the left-hand side show the molar ratio of aptamer:FPhOBtz:quinine. Top spectrum shows a reference spectrum of MN4 bound to quinine in the absence of FPhOBtz. Spectra were acquired with an MN4 concentration of 1.4 mM in 140 mM NaCl, 10 mM $Na_xH_yPO_4$, pH 6.8, 10% ^2H_2O−90% H_2O at 5 °C. Emergence of the G31 resonance for quinine-bound MN4 is highlighted by the red dot.

FPhOBtz: A Universal 3WJ Binder and Use in Host−Guest Biosensing Applications as a Label-Free Reporter. The specificity of FPhOBtz for the 3WJ binding domain and subsequent displacement by 10 equiv of quinine was compared to the performance of commercially available dyes that also contain the DNA binding Btz acceptor moiety (Figure 9A). PicoGreen dye (Pico488, 0.5 μM) was added to MN4 (1 μM) to afford bright emission at 529 nm with an I_{rel} ≈ 800-fold that of the free dye in solution. However, addition of 10 equiv of quinine failed to displace the dye from the MN4 aptamer. The structurally related TO afforded a relatively small I_{rel} value (~100-fold light-up) and, like Pico488, displayed little change in fluorescence intensity upon addition of 10 equiv of quinine. Given that Pico488 binds to double-stranded DNA, it should bind to the stems of MN4. It is noteworthy that the Pico488 structural analogue SYBR Green I (SGI) has been utilized in a cocaine detection platform.[39] However, the platform requires exonuclease III (Exo III) digestion of the aptamer, which is inhibited through target binding to the 3WJ with SGI occupying the duplex regions as a signal reporter. The GQ-specific dye ThT also exhibited a relatively small light-up response to MN4 binding but was displaced from the aptamer upon addition of 10 equiv of quinine (~70% displacement, Figure 9A), suggesting that ThT does bind to the 3WJ binding domain of MN4. However, the light-up response of FPhOBtz to MN4 was far superior to the response by ThT, and the phenolate dye exhibited greater displacement mediated through quinine addition. Furthermore, ThT is noted for its turn-on response to other DNA motifs, notably GQ structures.[16] The turn-on fluorescence response of FPhOBtz upon binding to CABA (I_{rel} ≈ 180-fold) was compared to its emission in the presence of other nucleic acid samples (Figure S11). The samples tested included single-stranded DNA, RNA, a variety of duplexes (calf thymus (CT DNA), ATP aptamer, thrombin binding aptamer (TBA15) + 15mer complementary strand (Comp), DNA:RNA duplex hybrid), and GQ-folding oligonucleotides (TBA15, TBA29, human telomeric DNA (HTELO), ochratoxin A binding aptamer (OTA36) and insulin binding aptamer (Ins30)). The greatest light-up emission response of FPhOBtz for the alternative samples was observed for OTA36,[40] which provided a 26-fold increase. However, compared to the emission intensity response of FPhOBtz toward CABA and especially

https://doi.org/10.1021/acsabm.1c00431
ACS Appl. Bio Mater. 2021, 4, 6732−6741

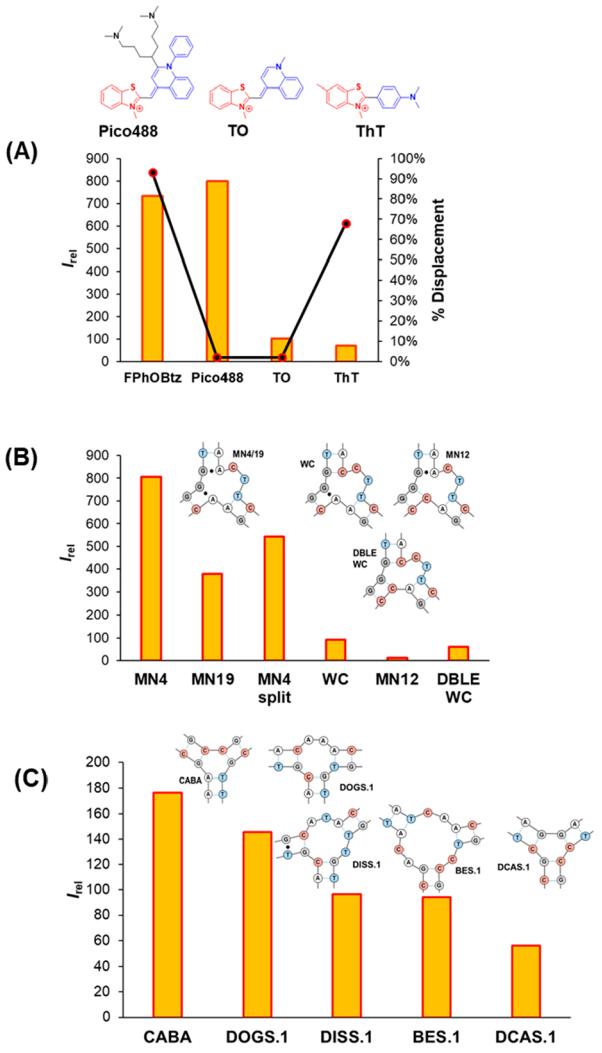

Figure 9. (A) Fluorescent light-up response (I_{rel}) of FPhOBtz upon binding MN4 versus I_{rel} for commercial dyes that also contain the Btz DNA binding acceptor moiety (bar graph), and perent displacement from MN4 upon addition of 10 equiv of quinine (line graph). (B) Fluorescent light-up response (I_{rel}) of FPhOBtz upon binding MN4 versus various MN4 variants. (C) Fluorescent light-up response (I_{rel}) of FPhOBtz upon binding CABA and other 3WJ-containing aptamers.

MN4 (734-fold), its fluorescence responses to the duplex, particularly CT DNA, and GQ structures were much weaker. This suggested the possibility that FPhOBtz could serve as a universal 3WJ binding light-up probe given its poor emission response to other nucleic acid secondary structures.

The emission intensity response of FPhOBtz was also examined in the presence of various MN4 variants (Figure 9B). The aptamer MN19 contains the same 3WJ binding domain as MN4, but stem 1 is reduced from 6 to 3 base pairs, which reduces the target (quinine and cocaine) binding affinity.[41] Given that the relative fluorescence response (I_{rel}) of FPhOBtz binding to the 3WJ binding domain correlates with binding affinity (i.e., $I_{rel} \approx 730$, $K_d = 0.42$ μM for MN4 versus $I_{rel} \approx 180$, $K_d = 9$ μM for CABA), the I_{rel} of ~375 for MN19 binding suggested decreased dye affinity, as noted for the targets. For the MN4 split, the A_3 loop of stem 2 (Figure 1) of MN4 was removed and the aptamer was divided into 11mer and 22mer oligonucleotides.[42] Addition of FPhOBtz to the 22mer provided essentially no emission response, while addition of the 11mer to the FPhOBtz-22mer mixture afforded an I_{rel} ~550-fold, implying that the binding free energy supplied by FPhOBtz is enough to bring the strands together to produce the 3WJ binding domain of MN4. Changes to the 3WJ region sequence had a dramatic impact on fluorescence response. The Watson–Crick (WC) variant contains a normal G:C base pair in stem 3, and the I_{rel} was reduced ~90-fold. The MN12 variant contains the normal G:C base pair in stem 1, and I_{rel} was only ~13-fold, while in the DBLE WC both G:A mismatches in stems 1 and 3 are replaced by G:C base pairs and I_{rel} was ~62-fold. Clearly, base sequence impacts FPhOBtz binding to the 3WJ binding domain of MN4, and it is informative that the same 3WJ region changes severely inhibit cocaine binding, with cocaine unable to bind MN12.[34]

Given the ability of FPhOBtz to serve as a label-free 3WJ reporter for target binding to MN4 and CABA, additional 3WJ aptamers were selected that further establish FPhOBtz as a universal 3WJ binder (Figure 9C). The aptamers selected (DOGS.1, DISS.1, BES.1, and DCAS.1) were generated by the Stojanovic laboratory to target a range of steroids.[43] The data presented in Figure 9C demonstrates the fluorescence light-up response of FPhOBtz to the four aptamers with a low I_{rel} of ~60-fold for DCAS.1 and a high of ~145-fold for DOGS.1. For BES.1, which binds selectively to estradiol, and DCAS.1, which binds to deoxycholic acid (DCA),[43] target-mediated displacement through loss of FPhOBtz emission provided 82% displacement by 50 equiv of estradiol and 77% by 50 equiv of DCA (Figure S12). These displacement values in the presence of 50 equiv of target matched the displacement data for cholic acid binding to CABA (Figure S8B).

As a final test, the ability of the host–guest biosensing assay to detect guest targets in human blood serum was determined. This biofluid was chosen because it contains high amounts of protein and proved to be a challenging matrix for cocaine detection using the UV-fluorescent reporter ATMND.[20] Considerable ATMND quenching at 405 nm occurred in serum due to competitive protein binding by the dye. Thus, the label-free platform employing ATMND could only be used in 2.5% serum.

For the present host–guest biosensing assay, the loss in fluorescence signal for 1 μM:2 μM FPhOBtz:aptamer in the presence of 10 μM quinine (Figure 7), 100 μM cocaine (Figure S8A), or 50 μM cholic acid (Figure S8B) in PBS buffer was compared to the corresponding signal loss in various concentrations of serum (2.5%, 5%, 10%, and 20%) mixed with PBS buffer. For quinine addition, only a 6.5% loss in signal change was observed between quinine detection in PBS buffer versus 20% serum (Figure S13). For cocaine detection, the loss in signal at 20% serum was still only 10.8% (Figure S14), while the loss in signal in 20% serum was 42.5% for cholic acid detection (Figure S15). Overall, these experiments confirmed the ability of the FPhOBtz dye to maintain its binding selectivity for the 3WJ binding domain of the DNA aptamers, especially MN4, in 20% serum. On the basis of these findings, the MN4/FPhOBtz label-free fluorescent assay can achieve detection limits of 650 nM, 20 μM, and 4.0 μM for quinine, cocaine, and cholic acid, respectively, in undiluted serum. While numerous aptamer-based assays have been reported for cocaine detection employing MN4, including colorimetric, electrochemical, capillary electrophoresis fluorescence, surface plasmon resonance,[44] compared to the only other published label-free fluorescent assay employing MN4/ATMND, which provides an LOD of 36 μM for cocaine detection in undiluted

https://doi.org/10.1021/acsabm.1c00431
ACS Appl. Bio Mater. 2021, 4, 6732–6741

serum,[20] the FPhOBtz probe represents a significant advancement for label-free sensing of targets that bind 3WJ DNA aptamers.

CONCLUSIONS

We have demonstrated the specific binding of the merocyanine dye FPhOBtz to the 3WJ of six DNA aptamers, establishing it as a universal 3WJ binding probe. The dye's preference for 3WJ binding is quite remarkable given that the aptamers also present duplex stems that are preferentially targeted by structurally related Btz-containing dyes, such as Pico488, TO, and SYBR Green I. For FPhOBtz binding to MN4 and CABA, which was studied in rigorous detail, the dye possesses greater binding affinity compared to two of the intended guests, cocaine and cholic acid. Thus, prebinding FPhOBtz to the 3WJ host can restrict cocaine and cholic acid entry depending on the concentration of dye:aptamer employed in the binding assay. The only guest with superior binding to the aptamer host than FPhOBtz was quinine, and FPhOBtz displacement mediated by quinine was efficient for excellent fluorescence read out for target detection (LoD ≈ 650 nM) in human blood serum. During our studies, a related phenolate merocyanine was employed to fluorescently stain nuclei and mitochondria in live cells,[45] highlighting the in vivo stability of these dye types. Thus, future collaborative studies will explore the in vivo biological activity of FPhOBtz given its potential to selectively target DNA 3WJs that are viewed as druggable targets. It is now anticipated that applications for phenolate merocyanines will greatly expand from their traditional roles as indicators of pH and solvent polarity. Their ability to specifically bind the DNA 3WJ secondary structure with an impressive turn-on fluorescence response (brightness ($\varepsilon\Phi_{fl}$) = 26 640 M^{-1} cm^{-1}) makes them highly useful for drug design (dye displacement by drug candidates) and biosensing and as efficient diagnostic tools during the assembly of DNA nanostructures.

EXPERIMENTAL SECTION

Materials and Methods. 2-Methylbenzothiazole, methyl iodide, 3-fluoro-4-hydroxy-benzaldehyde, quinine hemisulfate monohydrate, sodium cholate hydrate, cocaine hydrochloride solution (1.0 mg/mL in methanol), estradiol, deoxycholic acid, and DNA samples were obtained from commercial sources and used as received. Treatment of 2-methylbenzothiazole with methyl iodide (1.5 equiv) in acetonitrile at reflux was used to prepare *N*-methyl-2-methylbenzothiazolium iodide, as described previously.[23] NMR experiments were conducted on a 600 MHz Bruker Avance spectrometer equipped with an HCP triple-resonance probe. Mass spectra were acquired on an Agilent Q-TOF high-resolution (HRMS) instrument using an electrospray ionization source.

Merocyanine Dye Synthesis. FPhOBtz was synthesized by the Knoevenagel condensation reaction between 3-fluoro-4-hydroxy-benzaldehyde (1.60 mmol, 1.0 equiv) and *N*-methyl-2-methyl-benzothiazolium iodide (1.75 mmol, 1.1 equiv), catalyzed by piperidine (0.16 mmol, 0.1 equiv) in ethanol (0.2 M) at 80 °C using an oil bath, as outlined previously for the synthesis of other merocyanines.[23] Following precipitation with diethyl ether, the compound was isolated as a colored powder (FPhOBtz, 496 mg, 75%). ^{1}H NMR (DMSO-d_6, 600 MHz): δ 11.06 (br s, 1H), 8.40 (d, 1H, J = 8.0 Hz), 8.21 (d. 1H, J = 8.4 Hz), 8.13 (d, 1H, J = 15.8 Hz), 8.06 (m, 1H), 7.87 (m, 1H), 7.84 (d, 1H, J = 15.8 Hz), 7.78 (m, 1H), 7.70 (m, 1H), 7.07 (m, 1H), 4.32 (s, 3H). ^{13}C{^{1}H} NMR (DMSO-d_6, 150 MHz): δ 172.2, 153.1, 150.7, 148.4, 129.7, 129.3, 128.6, 128.0, 126.2, 124.6, 118.7, 117.1, 116.9, 111.7, 36.7. (ESI/Q-TOF) m/z: $[M]^+$ = calcd for $C_{16}H_{13}FNOS^+$, 286.0696; found, 286.0725.

UV−vis Measurements. All UV−vis spectra were obtained on a Cary 300-Bio UV−vis spectrophotometer. Stock solutions of FPhOBtz (2 mM) were prepared in DMSO. UV−vis titrations with 5 μM FPhOBtz in PBS buffer (pH 7.4) for MN4 and CABA binding were carried out at 25 °C with addition (0.25 equiv) of aptamer up to 20 μM (4 equiv) with manual mixing of the samples. The phenolic pK_a value for FPhOBtz was determined spectrophotometrically at 21 °C in 0.05 M aqueous buffer containing 0.2 M KCl, as previously outlined for other phenolic merocyanine dyes.[23]

Fluorescence Measurements. All fluorescence spectra were acquired on a Cary Eclipse Fluorescence spectrophotometer in quartz cells (108.002F-QS) with a path length of 10 × 2 mm at 20 or 25 °C. A 2 mM stock solution of FPhOBtz in DMSO was used. Fluorescence titrations with 1 μM FPhOBtz in PBS buffer (pH 7.4) were carried out with systematic addition up to 2 μM (2 equiv) MN4 and 2 μM CABA (2 equiv). The fluorescence spectra were recorded 2 min after manual mixing of the samples. The relative fluorescence quantum yields (Φ_{fl}) of unbound FPhOBtz and FPhOBtz·MN4 in PBS buffer at 20 °C were measured using quinine sulfate in 0.1 N sulfuric acid as the fluorescence standard solution.[46] Six samples in a concentration range from 0.2 to 10 μM unbound FPhOBtz were individually excited at 485 nm, and the integrated emission intensities were detected at 560 nm in a wavelength range of 500−600 nm. For the quantum yield measurements of FPhOBtz·MN4, FPhOBtz samples were mixed with 3-fold MN4 concentrations and the molar ratio of MN4:FPhOBtz was kept constant throughout the experiment. The photomultiplier tube voltage, signal-to-noise ratio, and spectral bandwidth parameters were also kept constant in all experiments. All MN4 samples were heated in a 95 °C water bath for 3 min and cooled in an ice−water bath for 5 min to allow the aptamer to anneal prior to each experiment. FPhOBtz·MN4 samples were individually excited at 540 nm, and the integrated emission intensities were detected at 580 nm in a wavelength range of 550−650 nm. The integrated emission intensities were plotted against the integrated excitation (absorption) intensities. The obtained linear slope was used to quantify the relative quantum yield values using the OriginPro 2016 software package.

Displacement experiments were carried out by first binding FPhOBtz to the aptamer forming the dye−DNA complex in PBS buffer and the subsequent displacement of FPhOBtz in response to addition of the target ligand (10 equiv of quinine, 100 equiv of cocaine, 50 equiv of cholic acid, estradiol, deoxycholic acid). The fluorescence spectra were recorded 2 min after manual mixing of the samples.

The fluorescence response of FPhOBtz (1 μM) to other DNA topologies (2 μM) was determined by adding various DNAs to 1 mL of 1 μM FPhOBtz in PBS buffer 7.4. The fluorescence reading was obtained 2 min after mixing. MN4 and CABA represented the 3WJ topology. Fluorescence emission was used to calculate the I_{rel} values.[13]

Isothermal Titration Calorimetry. ITC binding experiments were performed using a MicroCal VP-ITC instrument in a manner similar to what has been previously described.[25] The DNA was dissolved in ∼1 mL of ddH_2O per 1 micromole scale synthesis and exchanged 3 times against 1 M NaCl and then 4−6 times against ddH_2O. The MN4 cocaine binding aptamer samples were finally exchanged 3−4 times against the buffer (20 mM TRIS (pH 7.4), 140 mM NaCl, 5 mM KCl), and the CABA was exchanged against 10 mM sodium phosphate (pH 7.4), 140 mM NaCl, 5 mM KCl (PBS). The aptamer concentration was measured using UV spectroscopy and the known extinction coefficient provided by the manufacturer. Stock solutions of quinine and sodium cholate were prepared in the same buffer as their respective aptamers, while FPhOBtz was prepared in 100% DMSO.

Samples were degassed before analysis with a MicroCal Thermo Vac unit for 5 min. All experiments were corrected for the heat of dilution of the titrant. Titrations were performed with the aptamer samples in the cell and the ligand as the titrant in the needle. All aptamer samples were heated in a 95 °C water bath for 3−5 min and cooled in an ice water bath for at least 10 min prior to use in a binding experiment to allow the DNA aptamer to anneal in an intramolecular fashion. The binding experiments were performed at 15 °C with the

https://doi.org/10.1021/acsabm.1c00431
ACS Appl. Bio Mater. 2021, 4, 6732−6741

aptamer solution ranging from 20 to 50 μM using a ligand concentration of 0.312−1.3 mM. FPhOBtz was diluted to the experimental concentration with the buffer to a final DMSO concentration of 1% (v/v). DMSO was added to the aptamer solution and the reference cell at the same concentration to avoid buffer mismatch. All binding experiments consisted of an initial delay of 60 s, first injection of 2 μL, and 300 s delay. Subsequently, 34 injections of 8 μL were spaced every 300 s. The first point was removed from all data sets due to the different injection volume and delay parameters. ITC data were fit to a one-site binding model using the manufacturer provided Origin 7 software. ITC-based competition binding experiments were performed at 15 °C in their respective buffers containing 0.6% DMSO. This method used 20 μM aptamer with a 1.5-fold molar excess of bound ligand. A 0.52 mM solution of the second ligand was then titrated to a 5-fold molar excess. Data were fit to a competitive binding model provided by the Origin 7.0 software.

NMR Experiments. The MN4 sample was heated in boiling water for 1 min and then cooled in an ice−water bath for at least 5 min to favor intramolecular folding of the aptamer prior to performing NMR experiments. One-dimensional ^{1}H NMR spectra were acquired in 140 mM NaCl, 10 mM $Na_xH_yPO_4$ at pH 6.8 in 10% ^2H_2O/90% ^1H_2O at 5 °C in a manner described previously.[38] The concentration of the MN4 aptamer in the buffer was 1.4 mM at a volume of 600 μL. For the NMR experiments, the FPhOBtz dye was dissolved in DMSO-d_6 (99.96%). FPhOBtz was titrated into the MN4 sample to a 1:1 ratio of aptamer:ligand, bringing the final DMSO content of the sample to ∼5%. Two-dimensional ^{1}H−^{1}H NOESY was performed on a dye-bound MN4 sample with a mixing time (τ_m) of 200 ms. Water suppression for all experiments was achieved using excitation sculpting. Quinine−FPhOBtz competition experiments were performed using a 500 μM sample of MN4 in the previously described NMR buffer. For these experiments, quinine and FPhOBtz were each separately dissolved in DMSO-d_6. First, FPhOBtz was titrated into MN4 until a final molar ratio of 1:1 aptamer:FPhOBtz. The final DMSO content was ∼2% v/v. Next, quinine was titrated into the same sample to a final molar ratio of 1:1:3 aptamer:FPhOBtz:quinine with an ∼5% v/v final DMSO content.

Guest Detection in Serum. Human serum from human male AB plasma was purchased from Sigma-Aldrich, and various concentrations (2.5%, 5%, 10%, and 20%) were prepared in 1 mL vials containing standard 1 × PBS buffer solution (137 mM NaCl, 2.7 mM KCl, 8 mM Na_2HPO_4, and 2 mM KH_2PO_4, pH 7.4). To test the effects of serum on the initial dye signal we mixed FPhOBtz (1 μM) with the serum solutions followed by the addition of DNA, MN4, or CABA (2 μM) to the solution. Fluorescence measurements were performed after each step. The targets ([cocaine] = 100 μM, [quinine] = 10 μM, [cholic acid] = 50 μM) were then spiked into different dilutions of serum + DNA 3WJ + FPhOBtz, and the subsequent fluorescence signal change was obtained.

■ ASSOCIATED CONTENT

Supporting Information

The Supporting Information is available free of charge at https://pubs.acs.org/doi/10.1021/acsabm.1c00431.

UV−vis pK_a determination for FPhOBtz; solvatochromism and $E_T(30)$ correlation for FPhOBtz; pH influence on the fluorescence intensity of FPhOBtz·MN4; ITC thermogram for quinine binding to MN4; ITC thermogram for cholic acid binding to CABA; NOESY spectrum of MN4; histogram of ^{1}H NMR chemical shifts of free and bound MN4; fluorescence titration of target-mediated displacement from 3WJs; determination of LoD and LoQ; ITC-based competition binding experiments; ITC competition experiment results; I_{rel} for FPhOBtz binding to various DNA/RNA samples; target-mediated displacement by estradiol and DCA; detection of quinine in human serum; detection of cocaine in human serum; detection of cholic acid in human serum; ^{1}H NMR spectrum of FPhOBtz in DMSO-d_6; ^{13}C NMR spectrum of FPhOBtz in DMSO-d_6; positive-ionization HRMS of FPhOBtz (PDF)

■ AUTHOR INFORMATION

Corresponding Authors

Philip E. Johnson − *Department of Chemistry, York University, Toronto, Ontario M3J 1P3, Canada;* orcid.org/0000-0002-5573-4891; Email: pjohnson@yorku.ca

Richard A. Manderville − *Departments of Chemistry and Toxicology, University of Guelph, Guelph, Ontario N1G 2W1, Canada;* orcid.org/0000-0003-4035-8093; Email: rmanderv@uoguelph.ca

Authors

Abigail J. Van Riesen − *Departments of Chemistry and Toxicology, University of Guelph, Guelph, Ontario N1G 2W1, Canada*

Jennifer Le − *Departments of Chemistry and Toxicology, University of Guelph, Guelph, Ontario N1G 2W1, Canada*

Sladjana Slavkovic − *Department of Chemistry, York University, Toronto, Ontario M3J 1P3, Canada*

Zachary R. Churcher − *Department of Chemistry, York University, Toronto, Ontario M3J 1P3, Canada*

Aron A. Shoara − *Department of Chemistry, York University, Toronto, Ontario M3J 1P3, Canada;* orcid.org/0000-0002-5580-1273

Complete contact information is available at: https://pubs.acs.org/10.1021/acsabm.1c00431

Notes

The authors declare no competing financial interest.

■ ACKNOWLEDGMENTS

Financial support was provided by the Natural Sciences and Engineering Research Council (NSERC) of Canada (Discovery grants to P.E.J., 06381-2018, and R.A.M., 04621-2018).

■ REFERENCES

(1) Woods, K. C.; Martin, S. S.; Chu, V. C.; Baldwin, E. P. Quasi-Equivalence in Site-Specific Recombinase Structure and Function: Crystal Structure and Activity of Trimeric Cre Recombinase Bound to a Three-Way Lox DNA Junction. *J. Mol. Biol.* **2001**, *313*, 49−69.

(2) Duskova, K.; Lamarche, J.; Amor, S.; Caron, C.; Queyriaux, N.; Gaschard, M.; Penouilh, M.-J.; de Robillard, G.; Delmas, D.; Devillers, C. H.; Granzhan, A.; Teulade-Fichou, M.-P.; Chavarot-Kerlidou, M.; Therrien, B.; Britton, S.; Monchaud, D. Identification of Three-Way DNA Junction Ligands through Screening of Chemical Libraries and Validation by Complementary in Vitro Assays. *J. Med. Chem.* **2019**, *62*, 4456−4466.

(3) Dong, Y.; Yao, C.; Zhu, Y.; Yang, L.; Luo, D.; Yang, D. DNA Functional Materials Assembled from Branched DNA: Design, Synthesis, and Applications. *Chem. Rev.* **2020**, *120*, 9420−9481.

(4) Seo, H.; Ma, K. Y.; Tuttle, E. E.; Calderon, I. A. C.; Buskermolen, A. D.; Flask, C. A.; Clark, H. A. A DNA-Based MRI Contrast Agent for Quantitative pH Measurements. *ACS. Sens.* **2021**, *6*, 727−732.

(5) Zhang, L.; Guo, S.; Zhu, J.; Zhou, Z.; Li, T.; Li, J.; Dong, S.; Wang, E. Engineering DNA Three-Way Junction with Multifunctional Moieties: Sensing Platform for Bioanalysis. *Anal. Chem.* **2015**, *87*, 11295−11300.

(6) Yu, X.; Alkhamis, O.; Canoura, J.; Liu, Y.; Xiao, Y. Advances and Challenges in Small-Molecule DNA Aptamer Isolation, Characterization, and Sensor Development. *Angew. Chem., Int. Ed.* **2021**, *60*, 16800−16823.
(7) Li, F.; Lin, Y.; Le, C. Binding-Induced Formation of DNA Three-Way Junctions and Its Application to Protein Detection and DNA Strand Displacement. *Anal. Chem.* **2013**, *85*, 10835−10841.
(8) Stojanović, M. N.; Green, E. G.; Semova, S.; Nikić, D. B.; Landry, D. W. Cross-Reactive Arrays Based on Three-Way Junctions. *J. Am. Chem. Soc.* **2003**, *125*, 6085−6089.
(9) Yang, K.-A.; Chun, H.; Zhang, Y.; Pecic, S.; Nakatsuka, N.; Andrews, A. M.; Worgall, T. S.; Stojanovic, M. N. High-Affinity Nucleic-Acid-Based Receptors for Steroids. *ACS Chem. Biol.* **2017**, *12*, 3103−3112.
(10) Li, X.; Zhang, P.; Dou, L.; Wang, Y.; Sun, K.; Zhang, X.; Song, G.; Zhao, C.; Li, K.; Bai, Y.; Zeng, X.; Zhou, C.; Ying, B.; Chen, J.; Geng, J. Detection of Circulating Tumor Cells in Breast Cancer Patients by Nanopore Sensing with Aptamer-Mediated Amplification. *ACS Sens.* **2020**, *5*, 2359−2366.
(11) Du, Y.; Dong, S. Nucleic Acid Biosensors: Recent Advances and Perspectives. *Anal. Chem.* **2017**, *89*, 189−215.
(12) Manna, S.; Srivatsan, S. G. Fluorescence-Based Tools to Probe G-Quadruplexes in Cell-Free and Cellular Environments. *RSC Adv.* **2018**, *8*, 25673−25694.
(13) Deore, P. S.; Gray, M. D.; Chung, A. J.; Manderville, R. A. Ligand-Induced G-Quadruplex Polymorphism: A DNA Nanodevice for Label-Free Aptasensor Platforms. *J. Am. Chem. Soc.* **2019**, *141*, 14288−14297.
(14) Li, D.; Song, S. P.; Fan, C. H. Target-Responsive Structural Switching for Nucleic Acid-Based Sensors. *Acc. Chem. Res.* **2010**, *43*, 631−641.
(15) Lubitz, I.; Zikich, D.; Kotlyar, A. Specific High-Affinity Binding of Thiazole Orange to Triplex and G-Quadruplex DNA. *Biochemistry* **2010**, *49*, 3567−3574.
(16) Mohanty, J.; Barooah, N.; Dhamodharan, V.; Harikrishna, S.; Pradeepkumar, P. I.; Bhasikuttan, A. C. Thioflavin T as an Efficient Inducer and Selective Fluorescent Sensor for the Human Telomeric G-Quadruplex DNA. *J. Am. Chem. Soc.* **2013**, *135*, 367−376.
(17) Zipper, H.; Brunner, H.; Bernhagen, J.; Vitzthum, F. Investigations on DNA Intercalation and Surface Binding by SYBR Green I, Its Structure Determination and Methodological Implications. *Nucleic Acids Res.* **2004**, *32*, e103.
(18) Fürstenberg, A.; Julliard, M. D.; Deligeorgiev, T. G.; Gadjev, N. I.; Vasilev, A. A.; Vauthey, E. Ultrafast Excited-State Dynamics of DNA Fluorescent Intercalators: New Insight into the Fluorescence Enhancement Mechanism. *J. Am. Chem. Soc.* **2006**, *128*, 7661−7669.
(19) Stojanovic, M. N.; Landry, D. W. Aptamer-Based Colorimentric Probe for Cocaine. *J. Am. Chem. Soc.* **2002**, *124*, 9678−9679.
(20) Roncancio, D.; Yu, H.; Xu, X.; Wu, S.; Liu, R.; Debord, J.; Lou, X.; Xiao, Y. A Label-Free Aptamer-Fluorophore Assembly for Rapid and Specific Detection of Cocaine in Biofluids. *Anal. Chem.* **2014**, *86*, 11100−11106.
(21) Yang, Z.; Chen, Y.; Li, G.; Tian, Z.; Zhao, L.; Wu, X.; Ma, Q.; Liu, M.; Yang, P. Supramolecular Recognition of Three Way Junctions DNA by a Cationic Calix [3] Carbazole. *Chem. - Eur. J.* **2018**, *24*, 6087−6093.
(22) Wan, Q.; Chen, S.; Shi, W.; Li, L.; Ma, H. Lysosomal pH Rise During Heat Shock Monitored by a Lysosome-Targeting Near-Infrared Ratiometric Fluorescent Probe. *Angew. Chem., Int. Ed.* **2014**, *53*, 10916−10920.
(23) Van Riesen, A. J.; Johnson, R. E.; Al-Abdul-Wahid, S.; Liota, C.; Christyanton, A.; Manderville, R. A. Temperature Sensing of Thiolate Addition by Phenolate Merocyanine Dyes: Importance of the Quinone Methide Resonance Structure. *J. Org. Chem.* **2021**, *86*, 1583−1590.
(24) Stojanovic, M. N.; de Prada, P.; Landry, D. W. Aptamer-Based Folding Fluorescent Sensor for Cocaine. *J. Am. Chem. Soc.* **2001**, *123*, 4928−4931.
(25) Neves, M. A. D.; Reinstein, O.; Johnson, P. E. Defining a Stem Length-Dependent Binding Mechanism for the Cocaine-Binding Aptamer. A Combined NMR and Calorimetry Study. *Biochemistry* **2010**, *49*, 8478−8487.
(26) Kato, T.; Yano, K.; Ikebukuro, K.; Karube, I. Interaction of Three-Way DNA Junctions with Steroids. *Nucleic Acids Res.* **2000**, *28*, 1963−1968.
(27) Kato, T.; Yano, K.; Ikebukuro, K.; Karube, I. Bioassay of Bile Acids Using an Enzyme-Linked DNA Aptamer. *Analyst* **2000**, *125*, 1371−1373.
(28) Reinstein, O.; Yoo, M.; Han, C.; Palmo, T.; Beckham, S. A.; Wilce, M. C. J.; Johnson, P. E. Quinine Binding by the Cocaine-Binding Aptamer. Thermodynamic and Hydrodynamic Analysis of High-Affinity Binding of an Off-Target Ligand. *Biochemistry* **2013**, *52*, 8652−8662.
(29) Reichardt, C. Solvatochromic Dyes as Solvent Polarity Indicators. *Chem. Rev.* **1994**, *94*, 2319−2358.
(30) Singer, V. L.; Jones, L. J.; Yue, S. T.; Haugland, R. P. Characterization of PicoGreen Reagent and Development of a Fluorescence-Based Solution Assay for Double-Stranded DNA Quantitation. *Anal. Biochem.* **1997**, *249*, 228−238.
(31) Neves, M. A. D.; Slavkovic, S.; Churcher, Z. R.; Johnson, P. E. Salt-Mediated Two-Site Ligand Binding by the Cocaine-Binding Aptamer. *Nucleic Acids Res.* **2017**, *45*, 1041−1048.
(32) Slavkovic, S.; Churcher, Z. R.; Johnson, P. E. Nanomolar Binding Affinity of Quinine-Based Antimalarial Compounds by the Cocaine-Binding Aptamer. *Bioorg. Med. Chem.* **2018**, *26*, 5427−5434.
(33) Slavkovic, S.; Altunisik, M.; Reinstein, O.; Johnson, P. E. Structure-Affinity Relationship of the Cocaine-Binding Aptamer with Quinine Derivatives. *Bioorg. Med. Chem.* **2015**, *23*, 2593−2597.
(34) Neves, M. A. D.; Reinstein, O.; Saad, M.; Johnson, P. E. Defining the Secondary Structural Requirements of a Cocaine-Binding Aptamer by a Thermodynamic and Mutation Study. *Biophys. Chem.* **2010**, *153*, 9−16.
(35) Kato, T.; Takemura, T.; Yano, K.; Ikebukuro, K.; Karube, I. In Vitro Selection of DNA Aptamers which bind to Cholic Acid. *Biochim. Biophys. Acta, Gene Struct. Expression* **2000**, *1493*, 12−18.
(36) Churcher, Z. R.; Garaev, D.; Hunter, H. N.; Johnson, P. E. Reduction in Dynamics of Base Pair Opening upon Ligand Binding by the Cocaine-Binding Aptamer. *Biophys. J.* **2020**, *119*, 1147−1156.
(37) Churcher, Z. R.; Neves, M. A. D.; Hunter, H. N.; Johnson, P. E. Comparison of the Free and Ligand-Bound Imino Hydrogen Exchange Rates for the Cocaine-Binding Aptamer. *J. Biomol. NMR* **2017**, *68*, 33−39.
(38) Bottari, F.; Daems, E.; de Vries, A.-M.; Van Wielendaele, P.; Trashin, S.; Blust, R.; Sobott, F.; Madder, A.; Martins, J. C.; De Wael, K. Do Aptamers Always Bind? The Need for a Multifaceted Analytical Approach When Demonstrating Binding Affinity between Aptamer and Low Molecular Weight Compounds. *J. Am. Chem. Soc.* **2020**, *142*, 19622−19630.
(39) Wang, Z.; Yu, H.; Canoura, J.; Liu, Y.; Alkhamis, O.; Fu, F.; Xiao, Y. Introducing Structure-Switching Functionality into Small-Molecule-Binding Aptamers via Nuclease-Directed Truncation. *Nucleic Acids Res.* **2018**, *46*, e81.
(40) Cruz-Aguado, J. A.; Penner, G. Determination of Ochratoxin A with a DNA Aptamer. J. *J. Agric. Food Chem.* **2008**, *56*, 10456−10461.
(41) Neves, M. A. D.; Shoara, A. A.; Reinstein, O.; Abbasi Borhani, O.; Martin, T. R.; Johnson, P. E. Optimizing Stem Length To Improve Ligand Selectivity in a Structure-Switching Cocaine-Binding Aptamer. *ACS Sens.* **2017**, *2*, 1539−1545.
(42) Yu, H.; Canoura, J.; Guntupalli, B.; Lou, X.; Xiao, Y. A Cooperative-Binding Split Aptamer Assay for Rapid, Specific and Ultra-Sensitive Fluorescence Detection of Cocaine in Saliva. *Chem. Sci.* **2017**, *8*, 131−141.
(43) Yang, K.-A.; Pei, R.; Stefanovic, D.; Stojanovic, M. N. Optimizing Cross-reactivity with Evolutionary Search for Sensors. *J. Am. Chem. Soc.* **2012**, *134*, 1642−1647.

https://doi.org/10.1021/acsabm.1c00431
ACS Appl. Bio Mater. 2021, 4, 6732−6741

(44) Neves, M. A. D.; Blaszykowski, C.; Bokhari, S.; Thompson, M. Ultra-High Frequency Piezoelectric Aptasensor for the Label-Free Detection of Cocaine. *Biosens. Bioelectron.* **2015**, *72*, 383−392.
(45) Yang, R.; He, X.; Niu, G.; Meng, F.; Lu, Q.; Liu, Z.; Yu, X. A Single Fluorescent pH Probe for Simultaneous Two-Color Visualization of Nuclei and Mitochondria and Monitoring Cell Apoptosis. *ACS Sens.* **2021**, *6*, 1552−1559.
(46) Würth, C.; Grabolle, M.; Pauli, J.; Spieles, M.; Resch-Genger, U. Relative and Absolute Determination of Fluorescence Quantum Yields of Transparent Samples. *Nat. Protoc.* **2013**, *8*, 1535−1550.

https://doi.org/10.1021/acsabm.1c00431
ACS Appl. Bio Mater. 2021, 4, 6732−6741